



Calhoun: The NPS Institutional Archive
DSpace Repository

Theses and Dissertations

1. Thesis and Dissertation Collection, all items

1994-09

The IR missile (spin-scan and con-scan seekers) countermeasures

Chang, Ting Li

Monterey, California. Naval Postgraduate School

<http://hdl.handle.net/10945/30834>

This publication is a work of the U.S. Government as defined in Title 17, United States Code, Section 101. Copyright protection is not available for this work in the United States.

Downloaded from NPS Archive: Calhoun



<http://www.nps.edu/library>

Calhoun is the Naval Postgraduate School's public access digital repository for research materials and institutional publications created by the NPS community. Calhoun is named for Professor of Mathematics Guy K. Calhoun, NPS's first appointed -- and published -- scholarly author.

Dudley Knox Library / Naval Postgraduate School
411 Dyer Road / 1 University Circle
Monterey, California USA 93943

NAVAL POSTGRADUATE SCHOOL MONTEREY, CALIFORNIA



THESIS

THE IR MISSILE (SPIN-SCAN AND CON-SCAN SEEKERS) COUNTERMEASURES

by

Ting Li Chang

September, 1994

Thesis Advisor:

Alfred W. Cooper

Thesis
C37175

Approved for public release; distribution is unlimited.

DUDLEY KNOX LIBRARY
NAVAL POSTGRADUATE SCHOOL
MONTEREY CA 93943-5101

REPORT DOCUMENTATION PAGE

Form Approved OMB No. 0704-0188

Public reporting burden for this collection of information is estimated to average 1 hour per response, including the time for reviewing instruction, searching existing data sources, gathering and maintaining the data needed, and completing and reviewing the collection of information. Send comments regarding this burden estimate or any other aspect of this collection of information, including suggestions for reducing this burden, to Washington Headquarters Services, Directorate for Information Operations and Reports, 1215 Jefferson Davis Highway, Suite 1204, Arlington, VA 22202-4302, and to the Office of Management and Budget, Paperwork Reduction Project (0704-0188) Washington DC 20503.

1. AGENCY USE ONLY (Leave blank)	2. REPORT DATE September, 1994	3. REPORT TYPE AND DATES COVERED Master's Thesis	
4. TITLE AND SUBTITLE THE IR MISSILE (SPIN-SCAN AND CON-SCAN SEEKERS) COUNTERMEASURES (U)		5. FUNDING NUMBERS	
6. AUTHOR(S) Chang, Ting Li			
7. PERFORMING ORGANIZATION NAME(S) AND ADDRESS(ES) Naval Postgraduate School Monterey CA 93943-5000		8. PERFORMING ORGANIZATION REPORT NUMBER	
9. SPONSORING/MONITORING AGENCY NAME(S) AND ADDRESS(ES)		10. SPONSORING/MONITORING AGENCY REPORT NUMBER	
11. SUPPLEMENTARY NOTES The views expressed in this thesis are those of the author and do not reflect the official policy or position of the Department of Defense or the U.S. Government.			
12a. DISTRIBUTION/AVAILABILITY STATEMENT Approved for public release; distribution is unlimited		12b. DISTRIBUTION CODE *A	
13. ABSTRACT (maximum 200 words) In the combat scenario where the infrared missile is an almost continuous threat during the operation, fighter aircraft are currently quite susceptible to being killed in attacks by infrared missiles. Theoretical analysis applied to an encounter simulation seems to indicate that it is possible to use the infrared Active Jammer and the expendable decoy (flare) to defeat the infrared missile (spin-scan and con-scan seekers). The theoretical analysis of a simplified case of a spin-scan and con-scan reticle with amplitude modulation, frequency modulation and phase modulation leads to expressions for the targets' positions, as seen by the missile seeker, under no-jamming condition. The signal waveforms consist of target radiation power falling on the reticle and the reticle modulation function. We apply signal processing techniques to the modulated signal to determine the tracking error rate under no-jamming, active jamming and flare jamming different conditions, and by comparing with the unjammed tracking error rate, to determine the differences and effectiveness of jamming. The analytical result is simulated by means of a simulation program (MATLAB), which evaluates the change in the missile LOS (line of sight) rotation rate and the impact on the missile guidance operation. The analysis indicated successful jamming in the different jamming source situations. Following the jamming analysis, one can use the result to do further operational analysis as in OT&E (operation test and evaluation) and to evaluate the operational effectiveness of the jammers and to develop operational tactics to further increase the survivability of the fighter aircraft in the combat situation.			
14. SUBJECT TERMS Infrared missile (spin-scan and con-scan seekers) countermeasure, aircraft survivability		15. NUMBER OF PAGES 80	
		16. PRICE CODE	
17. SECURITY CLASSIFICATION OF REPORT Unclassified	18. SECURITY CLASSIFICATION OF THIS PAGE Unclassified	19. SECURITY CLASSIFICATION OF ABSTRACT Unclassified	20. LIMITATION OF ABSTRACT UL

NSN 7540-01-280-5500

Standard Form 298 (Rev. 2-89)
Prescribed by ANSI Std. Z39-18 298-102

Approved for public release; distribution is unlimited.

THE IR MISSILE (SPIN-SCAN AND CON-SCAN SEEKERS)
COUNTERMEASURES

by

Ting Li Chang
Lieutenant Colonel, Republic of China Air Force
B.S., Republic of China Air Force Academy, 1981

Submitted in partial fulfillment
of the requirements for the degree of

MASTER OF SCIENCE IN SYSTEMS ENGINEERING


from the

NAVAL POSTGRADUATE SCHOOL
September 1994


Author:


Ting Li Chang

Approved by:


Alfred W. Cooper, Thesis Advisor


Alfred W. Cooper, Second Reader


Frederic H. Levien, Chairman
Electronic Warfare Academic Group

thesis
C37795
C.2

ABSTRACT

In the combat scenario where the infrared missile is an almost continuous threat during the operation, fighter aircraft are currently quite susceptible to being killed in attacks by infrared missiles. Theoretical analysis applied to an encounter simulation seems to indicate that it is possible to use the infrared Active Jammer and the Expendable Decoy (flare) to defeat the infrared missile (spin-scan and con-scan seekers).

The theoretical analysis of a simplified case of a spin-scan and con-scan reticle with amplitude modulation, frequency modulation and phase modulation leads to expressions for the targets' positions, as seen by the missile seeker, under no-jamming condition. The signal waveforms consist of target radiation power falling on the reticle and the reticle modulation function. We apply signal processing techniques to the modulated signal to determine the tracking error rate under no-jamming, active jamming and flare jamming different conditions, and by comparing with the unjammed tracking error rate, to determine the differences and effectiveness of jamming. The analytical result is simulated by means of a simulation program (MATLAB), which evaluates the change in the missile LOS (line of sight) rotation rate and the impact on the missile guidance operation. The analysis indicated successful jamming in the different jamming source situations.

Following the jamming analysis, one can use the result to do further operational analysis as in OT&E (operation test and evaluation) and to evaluate the operational effectiveness of the jammers and to develop operational tactics to further increase the survivability of the fighter aircraft in the combat situation.

TABLE OF CONTENTS

I.	INTRODUCTION	1
A.	BACKGROUND	1
B.	SCOPE	1
C.	GENERAL SCENARIO	2
II.	THE AIRCRAFT IR SIGNATURE CHARACTERISTICS	3
A.	GENERAL INFRARED SIGNATURE FACTORS	3
1.	Jet Engine Signature Approximation	4
2.	Plume Radiation	5
3.	Aerodynamic Heating	6
4.	Solar Reflection	7
5.	Earthshine	8
B.	ATMOSPHERIC TRANSMISSION	9
C.	INFRARED SIGNATURE IN THE MISSION PROFILE	9
III.	THE INFRARED MISSILE SYSTEM	10
A.	AIRFRAME AND PROPULSION	10
B.	GUIDANCE AND STEERING	10
C.	IR MISSILE SEEKER	12
1.	Sensor	12

2. Seekers	12
a. Spin-Scan Seeker	13
b. Con-Scan Seeker.	15
IV. THE FALSE TARGET SIGNAL	17
A. INFRARED FLARES	17
1. Flare Intensity	17
2. Flare Ejection	18
B. ACTIVE IR JAMMER	18
V. SPIN-SCAN SEEKERS VS. FLARE AND IR JAMMER	19
A. BACKGROUND TO THE ANALYSIS	19
B. ANALYSIS	19
C. THE ACTIVE IR JAMMER	20
1. Target And Jamming Signal Seen By The Seeker.	20
2. The Tracking Error Signal Output	22
a. The Seeker With No Jamming	26
b. The Seeker Under Jamming Condition	27
(1) Jamming Power Fixed And Modulation Frequency Varied	27
(2) Jamming Power Varied And Modulation Frequency Fixed	29
(3) Jamming Power And Modulation Frequency Varied	31
D. FLARE JAMMING	34
1. Target And Flare Signal Seen By The Seeker	34
2. The Tracking Error Signal Output	35

E.	COMMENT AND RESULT	41
VI.	CON-SCAN SEEKERS VS. FLARE AND IR JAMMER	42
A.	BACKGROUND TO THE ANALYSIS	42
B.	ANALYSIS	42
C.	FLUX SIGNAL	44
D.	CON-SCAN SEEKER WITH NO JAMMING	45
E.	CON-SCAN SEEKER UNDER ACTIVE IR JAMMING	49
1.	Target And Jamming Signal Seen By The Seeker	49
2.	The Tracking Error Signal Output	51
a.	The Jamming Modulation Frequency Same As The Reticle Modulation Frequency	52
b.	The Jamming Modulation Frequency Different From The Reticle Modulation Frequency	54
F.	CON-SCAN SEEKER UNDER FLARE JAMMING	59
G.	COMMENT AND RESULT	64
VII.	CONCLUSION	66
	APPENDIX A SAMPLE OF THE SIMULATION PROGRAM	67
	LIST OF REFERENCES	69
	INITIAL DISTRIBUTION LIST	71

ACKNOWLEDGMENT

The author would like to acknowledge the financial support of this research by the Naval Postgraduate School Direct Funded Research Program through E.W. Academic group.

The author wants to thank Prof. A.W. Cooper for his guidance and patience during the work in performing this Thesis.

Finally, I thank most of all my Parents and my wife, Ruey-Chen, for their encouragement and love and my two lovely sons, Chun-Po and Chun-Chieh, who received little time and attention over many past months.

I. INTRODUCTION

A. BACKGROUND

Aircraft on an operational mission will not only be threatened by surface to air missiles but they will also be threatened by air-to-air missiles, which include missiles with many different guidance systems. In the past experience we find that the IR missile is the most efficient weapons threat to the aircraft.

B. SCOPE

This thesis will address a particular aspect of this threat - the threat by the infrared guided missile. This is because IR missiles are rather successful, as observed in the last 30 years, the kills of aircraft by IR missiles almost reach to 93% of the total compared to 5% for the radar missile and Gunfire.

For this thesis, we will consider aircraft that are already deployed, therefore the scope of survivability enhancement by vulnerability reduction is more limited than increasing survivability by susceptibility reduction.

Hence we will concentrate on the easier task of finding measures to reduce the susceptibility of these aircraft to being hit by an IR missile. Due to US government restrictions on dissemination of security-sensitive information, this thesis will be constrained to a more generic treatment of the problem.

C. GENERAL SCENARIO

In this thesis, it is assumed that the launch platform of the IR missile can reach a position such that the aircraft is within the acquisition range and in the range envelope of the missile. The aircraft is unassisted by other aircraft and lacks the capability to run away from the threat, but the pilot will know that the missile is already fired.

Since IR missiles are fire and forget weapons, multiple IR missiles can attack the same target. Therefore, this threat must also be handled. However, we will also assume that the multiple IR missile are the same type, during one attack.

II. THE AIRCRAFT IR SIGNATURE CHARACTERISTICS

A characterization of the aircraft in terms of the factors significant to the IR missile countermeasure problem is as follows:

A. GENERAL INFRARED SIGNATURE FACTORS

The IR signature of an aircraft is dependent, to various degree, on a number of factors. Various energy sources cause heating of the aircraft, and also reflect off aircraft surfaces.

For spatially unresolved targets, the total spectral radiant intensity is the quantity of most utility and is expressed as the sum of the individual contributing spectral radiant intensities:

$$I_t(\lambda) = I_p(\lambda) + I_h(\lambda) + I_n(\lambda) + I_s(\lambda) + I_e(\lambda) + I_q(\lambda) \quad (1)$$

here sub t represents the target total IR radiant intensity of interest;

p represents the target plume IR radiant intensity of interest;

h represents the target hot engine IR radiant intensity of interest;

n represents the target cowl and nozzle IR radiant intensity of interest;

s represents the target reflected solar IR radiant intensity of interest;

e represents the Earthshine IR radiant intensity of interest;

q represents the target skin aerodynamic heating IR radiant intensity of interest

In the subsequent sections, each of components of target IR radiant intensity is described:

1. Jet Engine Signature Approximation.

Jet engines can be divided into three classes: turbofans, turbojets, and ramjets. The total infrared emission from a jet engine consists of the plume, tailpipe, exhaust nozzle, and cowlings components. For a typical jet engine the emissivity ϵ for the nozzle and tailpipe components can be taken to be 0.9 and to be spectrally independent. The exhaust nozzle component temperature is related to a commonly reported engine parameter known as the exhaust gas temperature (EGT) read by a thermocouple just aft of the turbine. Exhaust gas temperature is a function of airspeed and altitude, and varies from 300 to 900 centigrade degrees for most jet engines. According to Hudson [Ref. 7], a rule-of-thumb relationship is:

$$T_e \approx 0.85EGT[^{\circ}C] \quad (2)$$

here T_e represents the exhaust nozzle temperature

The other required parameter for the calculation is the area of the nozzle, and the cowlings temperature must be estimated by considering heat transfer from the plume and removal due to freestream air flow on the exterior. Generally, even the most rudimentary estimate of jet-engine radiation requires a knowledge of the EGT, nozzle area and the projected areas in the direction of interest, emissivity of cowlings and plume, and temperature of cowlings and plume.

A general methodology to estimate target signature radiative components is as follows [Ref. 9]:

$$I_t(\lambda) = \sum_i I_i(\lambda) \quad (3)$$

$$I_i(\lambda) = \frac{W_{\lambda,i}}{\pi} A_i \quad (4)$$

$$W_{\lambda l} = \epsilon_l(\lambda, \theta, \phi) C_1 \lambda^{-5} \left[\exp\left(\frac{C_2}{\lambda T_l}\right) - 1 \right]^{-1} \quad (5)$$

where

$$C_1 = 3.1745 \times 10^4 \text{ W cm}^{-2} \mu\text{m}^{-1}$$

$$C_2 = 1.43879 \times 10^4 \mu\text{m K}$$

ϵ_l = directional spectral emissivity,

λ = wavelength in microns,

T_l = temperature of surface element.

Generally to calculate the total tailpipe exhaust nozzle radiant intensity from a jet engine, one can resort to the above equation for W_λ and integrate over wave-lengths, yielding the familiar Stefan-Boltzmann equation

$$I_n = \int_0^\infty W_\lambda d\lambda = \frac{\epsilon(\lambda, \theta, \phi) \sigma T_e^4}{\pi} \quad (6)$$

Generally, tailpipe and plume radiation is significantly stronger in the 3-5 μm atmospheric window than in the 8-12 μm band. For forward aspects, tailpipe radiation usually is not directly observable; Thus plume, skin emission, and reflected components dominate. In this case the 8-12 μm band may offer superior performance, however, a detailed analysis considering all operational requirements must be performed to validate such a choice.

2. Plume Radiation

The principal combustion products in the plume are carbon dioxide and water vapor, giving rise to characteristic molecular emission bands. Plume radiation is dependent on EGT, Mach number, afterburning, and altitude and viewing aspect. Accurate calculations are extremely complicated.

In general, W_λ varies from point to point within the plume because of temperature and emissivity variations, and thus, the radiant existence is itself spatially

variant. More generally, the radiant intensity from the i 'th element of the plume where $W_{\lambda i}$ can be assumed constant is :

$$I_i = \frac{A_i}{\pi} \int_{\lambda_1}^{\lambda_2} \epsilon(\lambda, \theta, \phi) W_{\lambda i} d\lambda \quad (7)$$

Calculation of the radiation from the plume requires some knowledge of the temperature distribution of the gases, which is a function of flight condition of the aircraft.

The afterburning engine plume consumes above five times the normal fuel and drastically increases thrust. The size of the plume increases substantially at high supersonic speeds. Because of low engine efficiency, the plume temperature may actually decrease. Nevertheless, if the temperature and emissivity can be estimated, the radiance from the plume can be calculated from the above equation. At higher temperatures during afterburning, the plume radiation spectra would be expected to broaden and the radiant intensity to increase by two to three orders of magnitude [Ref. 9]

3. Aerodynamic Heating

The emission from the target skin can be significant at frontal aspect in the 8-12 μ m region of the spectrum. This signal component can be written as [Ref. 9]

$$I_q = L_q(\lambda) \epsilon(\lambda, \theta, \phi) A_T \quad (8)$$

where

$L_q(\lambda)$ =radiance from skin;

$\epsilon(\lambda, \theta, \phi)$ =emissivity;

A_T =target surface area

The skin is aerodynamically heated according to the equation:

$$T_S = (1 + \frac{\gamma-1}{2} \beta M^2) T_a \quad (9)$$

where

T_s =skin temperature;

T_a =ambient temperature,

γ =ratio of the specific heats of air 1.4 at 25°C,

M=Mach number,

β =recovery factor (0.75 to 0.98).

4. Solar Reflection

The spectral target irradiance due to reflected sunlight can be obtained by multiplying the solar irradiance at the target by the target differential scattering cross section. Thus, [Ref 9]:

$$E_s = L_s \Omega_s T \rho \frac{d\sigma}{d\Omega} \quad (10)$$

where

L_s = radiance of sun,

Ω_s =solid angle subtended by the sun,

T= atmospheric transmittance from space to target,

ρ =reflectivity of target,

$\frac{d\sigma}{d\Omega}$ differential scattering cross section

After getting the spectral target irradiance due to reflected sunlight (E_s), then to calculate the average reflected solar radiant intensity as observed from space from a flat panel of metal with a Lambertian reflectance distribution generally one can use the form [Ref 9]:

$$I_s = \rho \frac{E_s A}{\pi} T \cos \theta \quad (11)$$

where

I_e = the average reflected solar radiant intensity,

A = area of the plate,

E_s =the average irradiance within the band ;

T = atmospheric band transmission from ground to space,

ρ =average reflectance of target material in the band,

θ =angle of incidence relative to the surface normal.

5. Earthshine

Reflected Earthshine is a minor component of the total contrast signature for viewing. However, as the view extends toward the horizon and the aspect becomes more side-on, the component increases. The total irradiance from Earthshine on a surface element of an aircraft is:

$$E_e(\theta, \Phi) = \pi L_e \sin^2 \frac{\theta}{2} \quad (12)$$

where

L_e = Earthshine radiance,

E_e =irradiance,

θ =angle between zenith and the surface normal.

The radiation scattered from the aircraft may be calculated as emission from a Lambertian source of area A . Accordingly, the scattered radiant intensity is:

$$I_e = \frac{\rho}{\pi} E_e(\theta, \phi) m \bullet n A \quad (13)$$

where

A = area of source,

ρ =reflectivity of surface,

m =direction of scattered radiation; n =surface normal.

B. ATMOSPHERIC TRANSMISSION

The atmosphere is well known to be a selective absorber [Ref. 2]. In the infrared bands, there are two windows, one at 3-5 μ m and the other at 8-14 μ m. Most of the detectors used in infrared missiles seekers are designed to work in these windows. Most detectors for air types are still using the 3-5 μ m wave band windows, since considerable radiant signature is found in the 3-5 μ m band.

C. INFRARED SIGNATURE IN THE MISSION PROFILE

The infrared signature of the aircraft in the takeoff and climbup phase will be greater than the cruise, on station, descent and landing phase, but in a mission operation phase, such as air combat, close air support, interception or air to ground attack, the infrared signature of the aircraft will be significantly higher. In those operation the pilot will always try to keep the aircraft operating at higher energy and higher speed, so it will cause the exhaust gas temperature to be higher, and the infrared signature to be higher. In the mission phase the infrared signature will vary by a factor two or more between those different modes of operation.

III. THE INFRARED MISSILE SYSTEM

A. AIRFRAME AND PROPULSION

Usually the IR missile has a cylindrical body with cruciform delta and trapezoidal wings and canards. The nose is blunt and transparent at the IR wave band of interest. Propulsion for Air to Air Missiles tends to be from single stage motors. Surface to Air Missiles are often two-staged motors, with a booster to get the missile up to flying speed rapidly and then a sustained motor for continuing the flight. The flight performance is characterized by the acceleration and velocity vectors attainable as a function of time, and the maximum ranges these give.

B. GUIDANCE AND STEERING

The IR missile guidance not only needs to consider the accurate homing tracking but also needs to consider the warhead capability to destroy the aircraft. When a warhead bursts in the vicinity of an aircraft, the fragments or penetrators are usually ejected uniformly around the missile axis, and the damage inflicted on the aircraft depends on the number and the location of the fragment impacts and on the terminal effect parameters, such as the fragment mass and impact velocity. In this situation, we assume the fragments travel on parallel paths and hit the aircraft in a random manner. The number of hits, n , required to destroy the aircraft capability, on the aircraft area presented at the aspect under consideration is given by [Ref 4]

$$n = \rho A_p \quad (14)$$

where ρ is the average number of fragments per unit area of fragment spray, known as the fragment spray density and A_p is the aircraft presented area at the aspect under consideration.

The fragment spray density at a distance S from the detonation point is given by:

$$\rho = \frac{N}{2\pi S^2 (\cos \phi_1 - \cos \phi_2)} \quad (15)$$

where the ϕ_1, ϕ_2 are the leading and trailing fragment dynamic trajectory angles with respect to a stationary target, and N is the total number of fragments in the warhead.

The equation defining the angles ϕ_1, ϕ_2 is:

$$\phi_i = \arctan \left[\frac{V_m \sin \theta + V_t \sin(\theta + \alpha_i)}{V_m \cos \theta + V_t \cos(\theta + \alpha_i) - V_i} \right] - \theta \quad (16)$$

where

V_i = target horizontal speed,

V_m = the speed of the missile,

θ = the elevation angle of the missile,

α = the leading and trailing fragment spray angles;

V_t = the average fragment speed with respect to a stationary warhead.

From above, the elevation angle of the missile (θ) should always get as close as possible to the target and provide the highest killing probability. To achieve an intercept using proportional navigation guidance, the missile must have a range closure and must control the line-of-sight rotation. To fly such a flight path, the missile seeker line-of-sight rate, relative to the target, must be zero. This keeps the seeker at a constant angle relative to the missile fuselage with the missile pulling lead on the target. A simplified relation that embodies proportional navigation can be stated as:

$$a_n = NV_m \dot{\sigma} \quad (17)$$

where

a_n = the commanded missile lateral acceleration in the guidance plane,

N = a proportionality constant,

V_m = the magnitude of the missile velocity vector,

$\dot{\sigma}$ = the line of sight rotation rate.

Steering is accomplished by one or a combination of aerodynamic surfaces or vectored thrust. To save mechanical complexity, some missile can only apply normal forces in one axis relative to their body coordinates, and depend on the rolling of the body to align the force in the direction desired.

C. IR MISSILE SEEKER

1. Sensor

Earlier generation detectors were made with lead sulphide. Indium antimonide is more widely used now. Lead sulphide detectors work around the 3 μm wave band whereas the detectivity of cooled indium antimonide peaks at around 5 μm . This allows the cooled indium antimonide detectors to work with radiation from all aspects with respect to the aircraft. This is in contrast to lead sulphide which can only work with the hot engine parts and engine plume [Ref. 2]

To accommodate the wide range in the scene and target irradiance as the missile flies towards its target, the detector is normally backed by an amplifier with Automatic Gain Control (AGC), so that the downstream processors have a normalized signal to work with. Significant parameters here are the attack and decay response times of the AGC and the saturation level.

2. Seekers

IR missile seekers have gone through a significant evolution in the past 30 years of development. The earliest seekers were simple spin-scan, rear-aspect, hot-spot trackers coupled to "bang-bang" control surfaces. These evolved into conical-scan trackers with all-aspect capability and proportional navigation guidance. Imaging seekers are under development in several countries, and we can expect several modes of imaging threats to be operational by the end of the decade. This thesis attempts to analyze jamming in the spin-scan seeker, and the con-scan seeker, so we need to understand both seekers to start the analysis. For both types, the target is focused to an image on the reticle plane, and the detector integrates the radiant energy passing through the reticle.

a. Spin-Scan Seeker

In the spin-scan seeker, energy emitted from the target is gathered by the seeker optical system and focused through a rotating reticle. The reticle chops the signal into a series of pulses, depending on the number of spokes and the spin-scan rate of the reticle. Chopping the signal allows the seeker to determine phase information (target direction) and the amplitude of the tracking error, and it assists in eliminating signal from extended background sources (clouds or the ground).

A reticle with half the disk 50% transmissive, tends to give for extended sources (such as clouds) a direct current (DC) signal while retaining the pulsed signal from point (target) sources. The 50% transmissive area yields a DC signal from the cloud; the extended cloud source is in more than one reticle sector at a time, thus giving a DC signal. The DC signal is then stripped to leave only the target pulses.

Most spin-scan seekers use amplitude modulation tracking. The detector output is fed into a band-pass filter which strips the DC signal from extended sources. The output of the band-pass filter is an interrupted sine wave (usually referred to

as "missile tone"). The signal is then passed through an envelope detector, which yields a square wave output. This is then fed into another band-pass filter, which strips the spin frequency of the reticle from the signal.

The resultant output signal is a sine wave. The amplitude of the sine wave corresponds to the magnitude of the tracking error, and the phase of the signal corresponds to the direction of the tracking error, as shown in Figure 1.

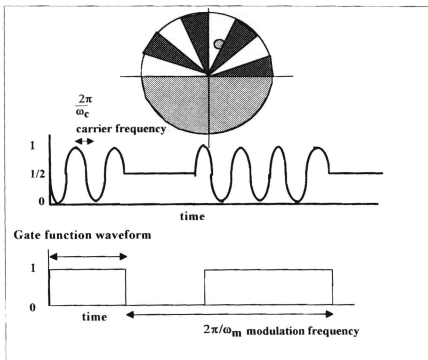


Figure 1. Spin-Scan Seeker Output Signal.

b. Con-Scan Seeker

In a typical con-scan seeker, the reticle is fixed and does not spin. Instead, the secondary mirror is tilted and spun. This causes the target image to be scanned in a circular path around the outer edge of the reticle. When the target is centered in the seeker scan, the detector gives a pulsed output similar to that of the spin-scan as shown in Figure 1. However, as the target leaves the center of the field of view, the output of the detector is a frequency modulation sine wave as shown in Figure 2. The depth of frequency modulation is directly proportional to the amount the target is displaced from the center of the seeker scan. The signal is processed by passing it through an FM discriminator whose output is an AM modulated signal with amplitude proportional to the amount of frequency modulation preset. The signal is passed through a demodulator to produce the target tracking error signal.

From this one can see that the con-scan seeker provides frequency modulation at small tracking errors and amplitude modulation at large tracking error when the nutation cycle of the target image is off the reticle during a part of scan cycle (see Figure 3).

The phase information in the tracking error provides the direction in which the center of the nutation circle moves relative to the reticle. If there is no LOS rotation rate (tracking error signal), the seeker reaches an equilibrium point, which means that the seeker is right on target.

If some LOS rotation rate is present, the nutation circle is offset from the center until the tracking error produces the necessary seeker driving torque to follow the LOS rotation rate. This is the principle of the equilibrium in the tracking loop i.e., the tracking point is displaced on the reticle until the torque generated to drive the seeker balances the LOS motion.

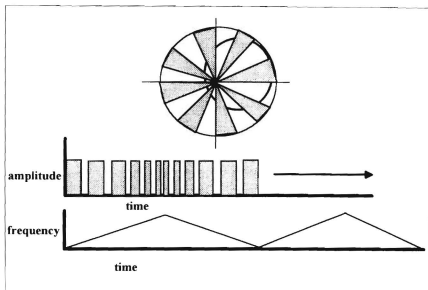


Figure 2. Con-Scan Seeker Under Small Tracking Error.

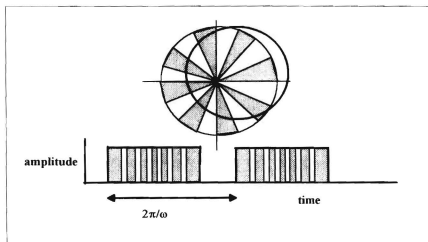


Figure 3. Con-Scan Seeker Under Large Tracking Error.

IV. THE FALSE TARGET SIGNAL

A. INFRARED FLARES

An IR flare is a self-protection device, designed to be ejected from an aircraft, that emits a large amount of radiation in the sensor bandwidth of an IR homing missile. It is supposed to be a more attractive target to the IR seeker. The seeker on an approaching IR missile will detect the presence of both the flare and the aircraft and hopefully will home in on the flare due to its IR signature. Since the flare is moving away from the aircraft, this may cause a miss distance sufficiently large to prevent a warhead detonation or leave the aircraft outside the fragment area.

1. Flare Intensity

There are several factors to be considered in utilization of flares. The flare must be of sufficient intensity (relative to the target signature) in the bandwidth of the IR detector to be seen as the more attractive target. It must be launched at the right time, in the right direction, and must reach full intensity quickly if it is to draw the missile away from the aircraft. It must also burn long enough to prevent the seeker from reacquiring the aircraft. The fact that the flare is a point source of IR intensity, whereas the aircraft and exhaust plume are distributed sources, may have an influence on the effectiveness of the flare in decoying the missile. The amount of influence will depend upon the type of target tracking in the missile.

In the flare energy spectra, the flare emissions do not match those of an aircraft with respect to spectral energy content. Because the flare must be very hot in order to develop enough radiant flux, most of the flare energy is in the short wavelengths below 2 μm . The flare intensity is affected by both the aircraft altitude and its velocity. There is a decrease in intensity for increasing altitude and a decrease in intensity for increasing velocity. The aircraft velocity has the most significant effect on the intensity, because the high velocity air passing around the flare reduces the size of the fireball and cools the surrounding air, thus reducing the intensity of the radiation.

2. Flare Ejection

Flares are ejected from a dispenser, and the flare should be ejected into nonturbulent airflow in order to minimize the decrease in intensity caused by velocity effects. Generally, flares are ejected down and slightly to the rear of the aircraft, thus this allows gravity to maintain the flare at the ejected velocity away from the aircraft and also draws the missile down and behind the departing aircraft. Flare ejection velocity should not be so low that the miss distance is insufficient to prevent warhead detonation, nor so high that the seeker will not respond to the rapidly moving flare and the lock-on will not be broken as the flare transits the seeker's field of view.

B. ACTIVE IR JAMMER

An active IR jammer modulates an IR source in order to provide misleading signals to the seeker. Against an amplitude modulation seeker, in addition to the AGC capture, the phase of the envelope variations can be manipulated by the infrared jammer and so the position vector determined by the seeker will be false.

V. SPIN-SCAN SEEKER VS. FLARE AND IR JAMMER

A. BACKGROUND TO THE ANALYSIS

The following analysis is derived from "*The IR and Electro-optical Systems Handbook*", volume 7, "*Countermeasure Systems*", Chapter 3 "*Active IR Countermeasure*" [Ref. 1]. In this chapter the writer considers jamming only by an active IR jammer, and did not deal with the variation of jamming effectiveness due to variation of amplitude and frequency of jammer modulation. In this thesis we consider not only active IR jamming but also the effectiveness of flare jamming, and we then compare jamming effectiveness for the two approaches.

B. ANALYSIS

In the following analysis, we only consider a general case, using the rising sun spin-scan seeker, of a target with collocated jammer that is modulated in time. In the flare case, we consider the flare has been ejected by the aircraft and the flare is modulated at the source frequency by the seeker. Here we deal with the jammer intensity and the flare intensity in the modulation output waveform, and we include the target position into the phase information, because those factors provide the tracking error to the control system. We assume that the IR signature has already propagated through the atmosphere into the detector. Then we concentrate on the linear signal processing unit to evaluate the tracking error rate provided to the control system. This should give us a clear result to determine the jamming effectiveness.

C. THE ACTIVE IR JAMMER

1. Target And Jamming Signal Seen By The Seeker

The target radiation seen by the detector is converted into a voltage or current and is processed through carrier amplifier, envelope detector, and precession amplifier circuits before the signal is applied to drive the seeker.

To get an insight into the jammer and seeker interaction, one should first define the reticle modulation function and the jammer modulation function, each of which can be represented by a Fourier series as shown in Figure 4. Each of the two modulations is periodic at a different angular frequency. The combination of them then can be processed.

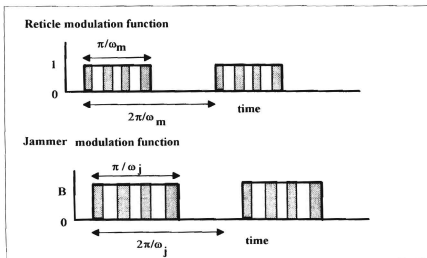


Figure 4. Jammer And Reticle Modulation Function.

The reticle modulation function for a generic reticle can be represented as

$$m_r(t) = \sum_{n=-\infty}^{\infty} c_n \exp(jn\omega_m t) \quad (18)$$

where

$$c_n = \frac{1}{T_m} \int_0^{T_m} m_r(t) \exp(-jn\omega_m t) dt \quad (19)$$

and $T_m = 2\pi/\omega_m$.

If the jammer waveform is also periodic at the angular frequency of ω_j , the jamming power incident on the seeker can be represented by:

$$P_j(t) = \sum_{k=-\infty}^{\infty} d_k \exp(jk\omega_j t) \quad (20)$$

where

$$d_k = \frac{1}{T_j} \int_0^{T_j} P_j(t) \exp(-jk\omega_j t) dt \quad (21)$$

and $T_j = 2\pi/\omega_j$.

It follows that the jamming source and the target source will both be modulated by the reticle, generally one can simplify the reticle modulation function to the form which is appropriate for example to the "rising sun" reticle:

$$m_r(t) = \frac{1}{2} [1 + \alpha m_i(t) \sin \omega_c t] \quad (22)$$

where

α = the ratio of the radius of the image location (or the tracking error) to

the radius of the reticle that provides a simplified measure of the

modulation efficiency;

$m_i(t)$ = a carrier gating function;

ω_c = the carrier frequency

and the Fourier series representation of $m_i(t)$ is:

$$m_t = \frac{1}{2} + \frac{2}{\pi} \sum_{n=0}^{\infty} \frac{(-1)^n}{2n+1} \sin[(2n+1)\omega_m t] \quad (23)$$

In this form the jamming modulation frequency and the jamming power can vary with time, for simplicity one can assume that the jammer has the same carrier frequency as the reticle and the jamming signal is also modulated by the reticle, the modulation frequency is ω_j , so one can represent the jamming power on the reticle in the form:

$$P_j(t) = \frac{B}{2} m_j(t) (1 + \sin \omega_c t) \quad (24)$$

where

$$m_j(t) = \frac{1}{2} + \frac{2}{\pi} \sum_{k=0}^{\infty} \frac{(-1)^k}{2k+1} \sin \{ (2k+1)[\omega_j t + \phi_j(t)] \} \quad (25)$$

B = the jamming peak power,

ϕ_j = the phase difference relative to $m_t(t)$.

2. The Tracking Error Signal Output

With this jamming signal seen by the seeker, the radiation power seen at the detector $P_d(t)$ may be represented by:

$$P_d(t) = A m_r(t) + P_j(t) m_r(t) \quad (26)$$

where A is the target radiation power falling on the reticle.

From above the P_d becomes :

$$P_d(t) = \frac{1}{2} [A + \frac{1}{2} B m_j(t) (1 + \sin \omega_c t)] [1 + \alpha m_r(t) \sin \omega_c t] \quad (27)$$

If this signal is then processed through a " carrier amplifier ", and assuming that the carrier amplifier passes signals at or near the carrier frequency only, the output of the carrier amplifier can be approximated by

$$S_c(t) \approx \alpha[A + \frac{1}{2}Bm_j(t)]m_i(t)\sin \omega_c t + \frac{1}{2}Bm_j(t)\sin \omega_c t \quad (28)$$

The envelope of the carrier modulation is then extracted in the form:

$$S_e(t) \approx \alpha Am_i(t) + \frac{B}{2}m_j(t)[1 + \alpha m_i(t)] \quad (29)$$

The envelope signal is further processed by a precession amplifier, which is tuned around the spin frequency ω_m . Assuming that ω_j is close to ω_m , the seeker driving signal is given by:

$$P_d(t) \approx \alpha(A + \frac{B}{4})\sin \omega_m t + \frac{B}{2}(1 + \frac{\alpha}{2})\sin[\omega_j t + \phi_j(t)] \quad (30)$$

This signal is used to apply torque to the spinning gyro of the seeker to correct the offset. The response can be discussed with the aid of the track error rate phasor diagram.

We will examine first the case of the spin-scan seeker with no jamming. With no jamming signal the driving signal takes the form,

$$P_d(t) = \alpha A \sin \omega_m t \quad (31)$$

and the phasor diagram shown as Figure 5:

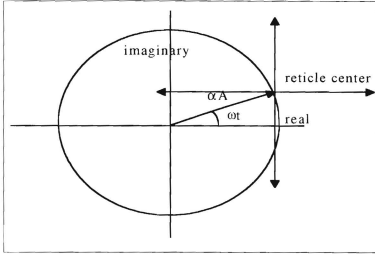


Figure 5. Spin-Scan Seeker Under No Jamming Tracking Error Phasor Diagram.

Without jamming the image point is driven toward the center along the imaginary direction with a rate proportional to αA , where it reaches an equilibrium point ($\alpha=0$).

With jamming condition:

$$P_d(t) \approx \alpha(A + \frac{B}{4})\sin \omega_m t + \frac{B}{2}(1 + \frac{\alpha}{2})\sin[\omega_j t + \phi_j(t)] \quad (32)$$

In the phasor diagram if we take the signal $\sin(\omega_m t + \phi)$ be the reference signal for $\phi=0$ in the horizontal direction then we get the detector error output in the phasor diagram as shown in Figure 6.

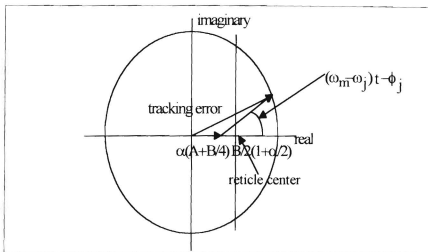


Figure 6. The Detector Error Output In The Phasor Diagram.

The tracking error rate phasor with jamming then becomes

$$P_d(t) \approx \alpha(A + \frac{B}{4}) + \frac{B}{2}(1 + \frac{\alpha}{2})\exp[j\beta(t)] \quad (33)$$

where $\beta = (\omega_m - \omega_j)t - \phi_j$

From the above phasor diagram, when the jammer is jamming the seeker the track error direction does not point correctly towards the reticle center. As the vector rotates in the phasor diagram for part of the revolution it may be directed towards the

center. But when the jamming power B is greater than $2\alpha A$, the tracking error vector is pulled away from center and if the revolution speed is low (ω_m and ω_j frequencies are very close) there is a chance that the seeker will break-lock, because the target is already out of the seeker field of view. It can be seen that for successful break-lock the requirement $J/S \geq 2\alpha$ should be met.

These results can be interpreted using the following simulations of the Tracking Error Rate Phasor carried out in the MATLAB programming language.

a. The Seeker With No Jamming

There are two variables A and α . The amplitude of the target, A , will depend on the angle at which the seeker looks at the target, so the amplitude of the target in the seeker is a random variable. Here we simplify it by taking an average value to represent the target amplitude seen by the seeker. The other variable, α , will be changed by the seeker tracking error; as the seeker drives the target toward the center, so α will decrease to zero. The simulated tracking error rate phasor diagram is shown in Figure 7.

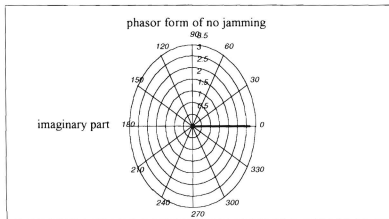


Figure 7. Spin-Scan Seeker Phasor Diagram Under No Jamming Condition.

The phasor diagram above shows us that the seeker will keep a constant value on the phase=0 direction to reduce the tracking error, till the output tracking error rate equal zero.

b. The Seeker Under Jamming Conditions

The tracking error function now takes the form

$$P_d(t) \approx \alpha(A + \frac{B}{4})\sin \omega_m t + \frac{B}{2}(1 + \frac{\alpha}{2})\sin[\omega_j t + \phi_j(t)] \quad (34)$$

Here, we see that there are four variables A, B, and ω_j , α . The amplitude of target and jammer, A and B, will depend on the angle at which the seeker looks at the target, because the jammer is collocated so that the amplitude of the target and the jammer power seen by the seeker are random variables. Here we simplify it by representing it by its average value. Also α will depend on the A and B values seen at the seeker location, so that only ω_j and ϕ_j remain as time dependent variables.

In the different simulation conditions, we assume that when the jammer first starts to get into the seeker the ϕ_j will be a fixed constant value.

(1) Jammer power fixed and modulation frequency varied. The first simulation will be conducted under the condition of jammer power fixed but the jamming modulation frequency varying. The 3D diagram and phasor diagram of tracking error rate are shown in Figures 8-1 and 8-2. A sample of the simulation program is shown in appendix.

spin-scan seeker tracking error rate under active IR jamming

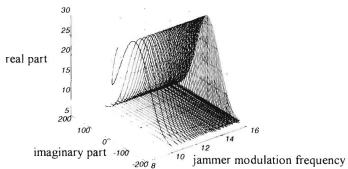


Figure 8-1. Tracking Error Rate Versus Jammer Modulation Frequency.

spin-scan seeker tracking error rate under active IR jamming phasor form

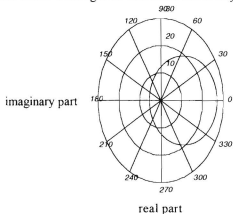


Figure 8-2. Phasor Representation Of Tracking Error Rate.

From Figure 8-1, we can see that the jammer angular frequency sweep will cause the seeker tracking error rate to change. Not only will the tracking error phase change, but the tracking error amplitude will change also. When the jammer angular frequency is not close to the seeker modulation frequency the tracking error rate will change rapidly. In this area if we try to break-lock the missile seeker, the chance of success will be lower than in the slow change area.

In the Figure 8-2 phasor diagram, break lock can occur only when the phasor can enter the region between -90 degree and $+90$ degree, i.e., the left hand side of the diagram of Figure 8-2. The phasor diagram of this figure shows that this can occur for the condition of J/S ratio greater than 2α . Under these circumstances missile seeker break-lock will occur if the tracking error rate changes slowly.

(2) Jamming power varied and modulation frequency fixed. The second simulation will be conducted under the condition of jammer power varied but the jamming modulation frequency fixed. The 3D diagram and phasor diagram of tracking error rate are shown in Figures 9-1 and 9-2.

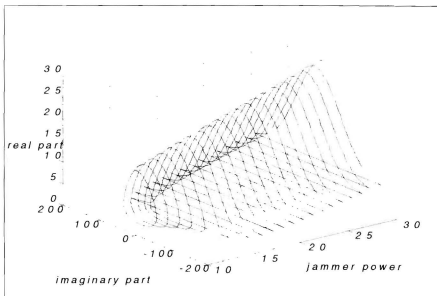


Figure 9-1. Spin-Scan Seeker Under Active Ir Jamming, Tracking Error Rate Versus Jamming Power.

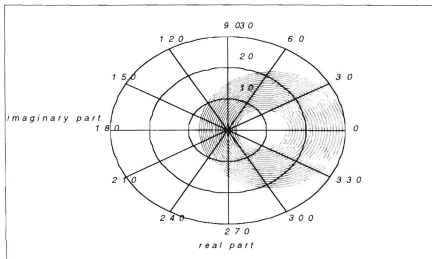


Figure 9-2. Tracking Error Rate Phasor Diagram.

From Figure 9-1, we can see that varying the jammer power will cause the seeker tracking error rate to change, not only in phase but also in amplitude. Since the jammer angular frequency is close to the seeker modulation frequency, the tracking error rate will change slowly; in this area the chance of causing break-lock of the missile seeker will be higher, but we should take the jammer power into consideration at same time.

In Figure 9-2 the phasor diagram shows us that as the jammer amplitude is varied from small power to higher power, so the phasor diagram circle moves from the center of the diagram to the left, and the rotation rate stays constant since the modulation frequency is kept fixed. From the phasor diagram, we also can see that when the jammer power ratio J/S is greater than 2α , the tracking error rate will cross over the center. Under this condition, again have the situation that the tracking error phase will pulled into the region to the left of center (i.e. between -90 and $+90$), which will cause the missile to break-lock, since the tracking error rate is changing slowly.

(3). Jammer power and modulation frequency varied. The third simulation is conducted under the condition of jammer power and modulation frequency varied. The 3D diagrams of jammer power versus tracking error output and jammer modulation frequency versus output tracking error signal are shown in Figures 10-1 and 10-2, the phasor diagram of tracking error rate as shown in Figure 10-3.

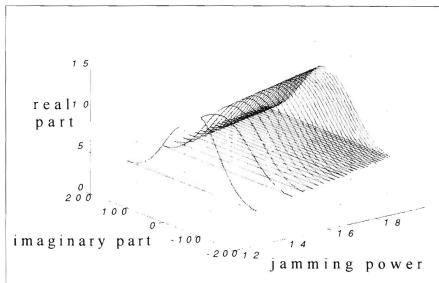


Figure 10-1. Spin-Scan Seeker Under Active Ir Jamming, Tracking Error Rate Versus Jamming Power.

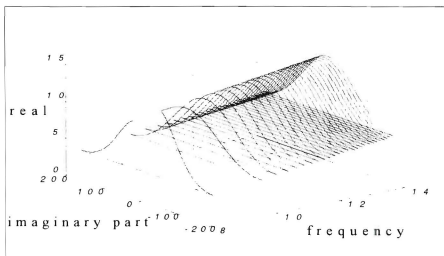


Figure 10-2. Spin-Scan Seeker Under Active Ir Jamming, Tracking Error Rate Versus Jamming Modulation Frequency.

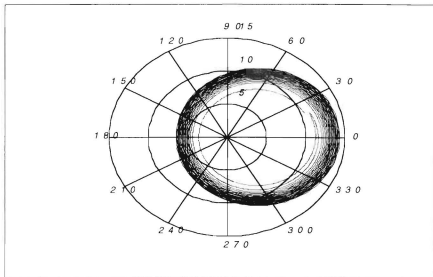


Figure 10-3. Spin-Scan Seeker Under Active Ir Jammer Jamming, Tracking Error Rate Phasor Diagram.

From Figures 10-1 and 10-2, we can see that the jammer power variation will cause the seeker tracking error amplitude to change, and variation of modulation frequency will also cause the tracking error phase to change.

Because the jammer angular frequency varies, the diagram shows us very clearly that when the jammer modulation frequency is close to the seeker modulation frequency, the tracking error rate will change slowly, and when the frequency is the same as the reticle modulation frequency, the phase will be delayed but when it decreases more the phase will change from positive to negative.

In the phasor diagram of Figure 10-3, the jammer amplitude is varied from small power to higher power so the phasor diagram circle moves from the center toward the perimeters and the rotation rate varies too, depending on the frequency difference between reticle and jammer.

D. FLARE JAMMING

1. Target And Flare Signal Seen By The Seeker

The target signal seen by the seeker will be similar to that shown above, however the flare will appear as a continuous source modulated by the reticle, so the radiation power seen at the detector $P_d(t)$ could be represented by:

$$P_d(t) = [Am_{rt}(t)] + [Bm_{rf}(t)] \quad (35)$$

here

$$m_{rt}(t) = \frac{1}{2}[1 + \alpha m_t(t)\sin \omega_c t] \quad (36)$$

$$m_{rf}(t) = \frac{1}{2}[1 + \beta m_f(t)\sin \omega_c t] \quad (37)$$

where

B= the flare jamming power,

α = the ratio of the radius of the image location (or the tracking error) to the radius of the reticle that provides a simplified measure of the modulation efficiency,

β = the ratio of the radius of the flare location (or the tracking error) to the radius of the reticle that provides a simplified measure of the modulation efficiency,

$m_t(t)$ = a target carrier gating function,

$m_f(t)$ = a flare carrier gating function,

ω_c = the carrier frequency

The Fourier series representations of $m_i(t)$ and $m_j(t)$ are:

$$m_i(t) = \frac{1}{2} + \frac{2}{\pi} \sum_{n=0}^{(-1)^n} \sin[(2n+1)\omega_m t] \quad (38)$$

$$m_j(t) = \frac{1}{2} + \frac{2}{\pi} \sum_{n=0}^{(-1)^n} \sin[(2n+1)\omega_m t + \phi_j] \quad (39)$$

here ϕ_j = the phase difference relative to $m_i(t)$.

2. The Tracking Error Signal Output

The target IR signal and the flare IR signal seen together by the detector, give a power to the detector that can be represented by:

$$P_d(t) = \left[\frac{A}{2} + \frac{A\alpha}{2} m_i(t) \sin \omega_c t \right] + \left[\frac{B}{2} + \frac{B\alpha}{2} m_j(t) \sin \omega_c t \right] \quad (40)$$

Assuming that the carrier amplifier passes signals only at or near the carrier frequency, the output of the carrier amplifier can be approximated by

$$S_c(t) = \left[\frac{A\alpha}{2} m_i(t) \sin \omega_c t \right] + \left[\frac{B\beta}{2} m_j(t) \sin \omega_c t \right] \quad (41)$$

The envelope of the carrier modulation is:

$$S_e(t) = \frac{A\alpha}{2} m_i(t) + \frac{B\beta}{2} m_j(t) \quad (42)$$

The envelope signal is further processed by a precession amplifier, which is tuned around the spin frequency ω_m . The seeker driving signal is then given by:

$$P(t) = \left[\frac{A\alpha}{2} m_i(t) \sin \omega_m t \right] + \left[\frac{B\beta}{2} m_j(t) \sin \omega_m t + \phi_j \right] \quad (43)$$

The driving signal torques a spinning gyroscope. The rotating magnet and the seeker torquing signal result in a seeker precession rate which shows in the phasor function. If in the phasor function we take the signal $\sin(\omega_m t)$ be the reference signal for $\phi=0$ in the horizontal direction, then we get the detector error signal output in the phasor diagram function in the form:

$$P(t) = \frac{A\alpha}{2} + \frac{B\beta}{2} \exp(j\phi(t)) \quad (44)$$

The phasor function above indicates that when the flare is jamming the seeker there is no equilibrium point in the center. The tracking error revolution will depend on the phase angle (ϕ) difference from the target. The change rate also depends on the separation between target and flare, since the flare will move away from the target the flare position seen by the seeker (β) will be changed and it will change the power ratio between the target and flare. When the flare power is greater than $\alpha A/\beta$, the tracking error vector is pulled into the left hand half of the diagram and if the separation speed between the target and flare is small there is a chance that the seeker will break-lock, because the target is already out of the seeker field of view. It follows from the analysis that successful break-lock requires the power ratio $J/S \geq \alpha/\beta$.

Here we show the simulation of flare jamming under two different conditions: first, fixed flare power, and second, varied flare power with other parameters fixed.

Figure 11-1 shows the variation of track error with phase delay relative to the target signal. The variation with β , the normalized target offset distance, is shown in Figure 11-2, while the trajectory of the track error rate is shown as Figure 11-3

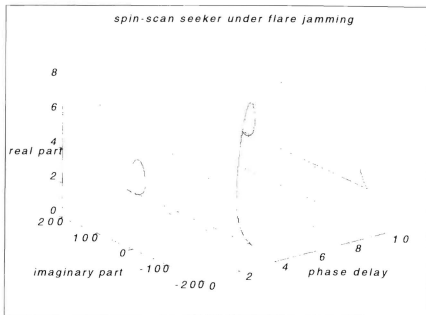


Figure 11-1. Spin-Scan Seeker Under Flare Jamming Track Error Rate Versus Phase Delay

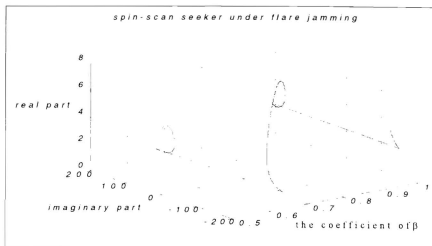


Figure 11-2. Spin-Scan Seeker Under Flare Jamming, Track Error Rate Versus Flare Radial Position.

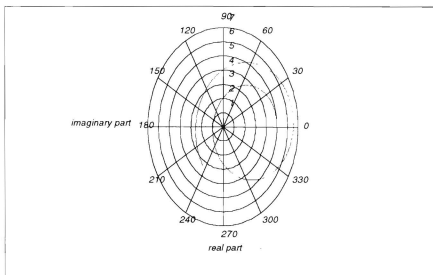


Figure 11-3 Spin-Scan Seeker Under Flare Jamming Phasor Diagram,
Trajectory Of Track Error Rate.

Inspection of the 3D plots and phasor diagram shows that if the missile is under flare jamming, with flare intensity very close to the target intensity, and if the flare leaves the target and the target separation from the flare is slow, (the image of the target seen by the seeker leads to the edge of the reticle), this will cause the seeker tracking error rate to become bigger and bigger.

In the second simulation condition the flare radiation power varies and the other conditions stay fixed. The plots of track error rate versus flare power and phase delay are shown as Figures 12-1, and 12-2 and the phasor diagram is shown as in Figure 12-3.

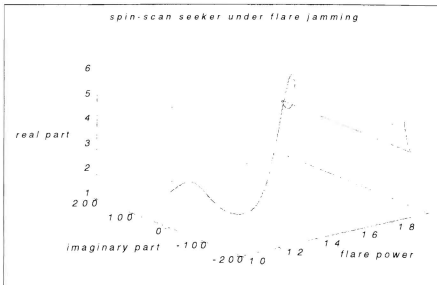


Figure 12-1. Spin-Scan Seeker Under Flare Jamming, Track Error Rate Versus Flare Power.

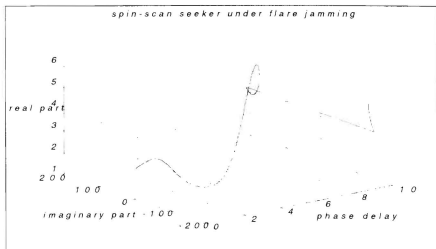


Figure 12-2. Spin-Scan Seeker Under Flare Jamming, Track Error Rate Versus Phase Delay.

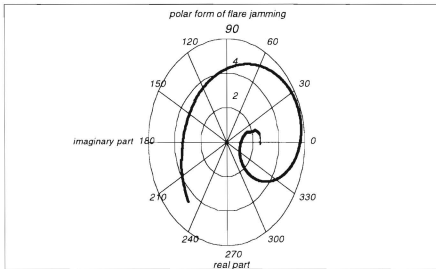


Figure 12-3. Spin-Scan Seeker Under Flare Jamming, Track Error Rate Phasor Diagram.

These simulations under two conditions indicate that when the seeker is jammed by the flare and the flare power is greater than $\alpha A/\beta$ then the missile seeker has a probability of being pulled towards the left of the seeker center, which will cause the seeker to break-lock. This simulation confirms that the flare is really efficient to counter the spin-scan seeker, when we drop the flare at the right time and perform the correct maneuvers with the aircraft we can successfully avoid the missile attack.

E. COMMENT AND RESULT

In the spin-scan seeker case we already simulated the three different conditions of no jamming, active IR jamming, and flare jamming. From the simulation results, we see that since the active IR jammer is collocated with the target, the false target image and the real target image will be seen by the seeker in the same location (same α). In attempting to jam the missile seeker one must consider the jammer power and the jamming modulation frequency; when the jamming modulation frequency is the same as the reticle modulation frequency, then the phase delay will be the important parameter for the jamming effectiveness.

The jamming power requirement depends not only the jamming power but also on the radial position coefficient α ; this will change the jammer power requirement from very small power to large power. In order to break-lock with the missile seeker, one should control the jammer modulation frequency and the jammer power; then there is a big chance to break-lock the missile.

In the flare case, since the flare will leave the aircraft, the target and flare positions determine the phase difference and different power coefficients (α , β), so we only need to consider target and flare. Once the trajectory of the flare and the aircraft moving moment are fixed then we can determine whether the flare can break-lock the missile or not. The simulation plot, under those particular conditions in which the jammer power is similar to the target power shows a high probability to break-lock the missile.

The theoretical analysis indicates the simplified case of a rising sun spin-scan seeker with AM modulation, to be successful jammed by both the active IR jammer and flare. The analysis done here is only a paper study, it should be evaluated in operating testing to ensure its validity, and the evaluation should be extended to application against different types of spin-scan seeker.

VI. CON-SCAN SEEKER VS. FLARE AND IR JAMMER

A. BACKGROUND TO THE ANALYSIS

This is a reticle in which the image is nutated over a stationary reticle. The resulting frequency modulation of the signal out of the detector can be processed to extract the position of the target relative to the reticle center.

The following analysis is derived from "*The IR and Electro-optical Systems Handbook*", volume 7, "*Countermeasure Systems*", Chapter 3 "*Active IR Countermeasure*". In this chapter the writer considers the active IR jammer jamming condition, but in this THESIS we not only consider the active IR jammer but also deal with the Flare jamming effectiveness, and then apply a MATLAB program to simulate different jamming conditions to evaluate the results and compare jamming effectiveness.

B. ANALYSIS

In the following analysis, we want to determine the apparent target position, as seen by the seeker, while under no jamming and jamming conditions. We only consider the general case of a target with collocated jammer, modulated in time. In the flare case, we consider the flare has been ejected by the aircraft and the flare is modulated at the same frequency by the seeker.

We deal with the jammer intensity and the flare intensity in the modulation output waveform, together with the target position coded into phase information, because those two parameters provide the tracking error to the control system. We assume that the IR target signature already passed through the atmosphere and into the detector, and concentrate in the linear signal processing on determination of the tracking error rate

provided into the control system. This output should clearly determine the jamming effectiveness.

In con-scan seekers, when the target is centered in the seeker, the detector gives a pulsed output similar to the spin-scan. The con-scan seeker provides frequency modulation at small tracking errors and amplitude modulation at large tracking error when the nutation cycle of the target image is off the reticle during a part of scan cycle. In this analysis we simplify the problem to analyze only the large error signal processing to evaluate the jamming effectiveness. This should give us a very clear comparison with the spin-scan seeker.

In the following analysis the phase information in the tracking error provides the direction in which the center of the nutation circle moves relative to the reticle. If there is no LOS rotation rate (tracking error signal), the target is inside the reticle and the seeker has reached an equilibrium point, this means that the seeker is right on target. If with some LOS rotation rate present because the nutation circle is offset from the center, then part of the scanning time it falls outside the reticle, as shown in Figure 13. The tracking error then produces the necessary seeker driving torque to follow the LOS rotation rate. This is the principle of the equilibrium in the tracking loop, i.e., the tracking point is displaced on the reticle until the torque generated to drive the seeker balances the LOS motion.

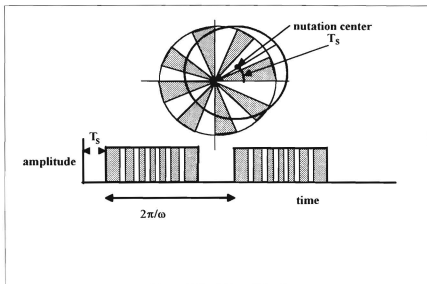


Figure 13. Con-Scan Modulation Output Signal, Nutation Circle Partly Off Reticle.

C. FLUX SIGNAL

In the real world the IR radiation signal strength seen by the seeker should depend on the target exhaust plume, hot engine IR radiant intensity, target cowling and nozzle IR radiant intensity, target reflected solar IR radiant intensity, Earthshine IR radiant intensity, skin aerodynamic heating IR radiant intensity, and the angle of the target. In this analysis we assume that the target IR radiation intensity seen by the seeker has a constant value, because it is a random variable one takes the average value to represent the radiation power to simplify the analysis.

Following this assumption we assume a uniformly illuminated target image moving in a circular path on the reticle. The time on the transmitting parts of the reticle will represent the total target radiation power seen by the reticle.

D. CON-SCAN SEEKER WITH NO JAMMING

Under the assumption that the target radiation power should have a constant value the constant power seen by the seeker would produce a periodic signal which can be represented by a Fourier series as shown in Figure 14.

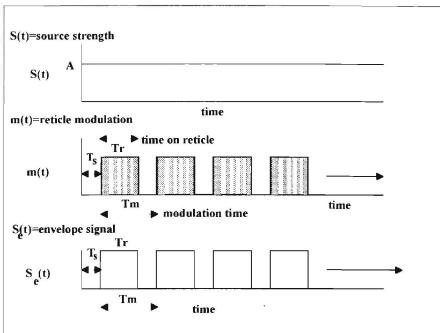


Figure 14. Schematic Of The Con-Scan Seeker Signal With No Jamming.

with these assumption the signal of the output may be represented by the following analysis.

$$S(t) = A \quad (45)$$

where A represented the target signal.

The target signal passed through the reticle modulation function can be written:

$$S(t) = Am(t) \quad (46)$$

where $m(t)$ can be represented by a Fourier series:

$$m(t) = \sum_{n=-\infty}^{\infty} d_n \exp[jn\omega_m(t - T_s)] \quad (47)$$

where

$$d_n = \frac{1}{T_m} \int_0^{T_m} \exp(-jn\omega_m t^*) dt \quad (48)$$

and

$$t^* = \frac{T_r}{T_m} t \quad (49)$$

T_r = time on reticle,

T_m = the scan period,

$\omega_m = 2\pi/T_m$,

T_s = The modulation delay of the target position (direction of the target),

d_n can also be written in the form:

$$d_n = \frac{j}{2\pi n} [\exp(-j2\pi n \frac{T_r}{T_m}) - 1] \quad (50)$$

The seeker tracking will be influenced by the signal frequency components at or near ω_m . An approximate form of this modulated waveform at the detector modulation can be written considering only the AC term and the fundamental frequency component of the modulation wave form, giving:

$$S_e(t) = -\frac{A}{\pi} [\sin(\omega_m(t - T_s) - 2\pi \frac{T_r}{T_m})] + \frac{A}{\pi} \sin \omega_m(t - T_s) \quad (51)$$

It should be noted that when T_r is greater than 0.5 in the modulation factor $m(t)$ of Figure 14, the signal is identical to that for 0 to 0.5. Therefore we need to analyze only for the range 0 to 0.5, as this gives a clear picture of tracking error output.

From above function we can see that in response to this drive signal, the seeker tracking loop will adjust T_r along the $\omega_m T_r$ direction to keep the average seeker tracking rate at zero. The corresponding drive signal is shown as Figure 15; when T_r / T_m reaches a value of 0.5 the tracking error signal is at its lowest, since then the seeker is right on target.

The MATLAB program has been used to simulate the tracking error output phasor diagram shown as Figures 16-1 and 16-2 with the resultant 3D diagram.

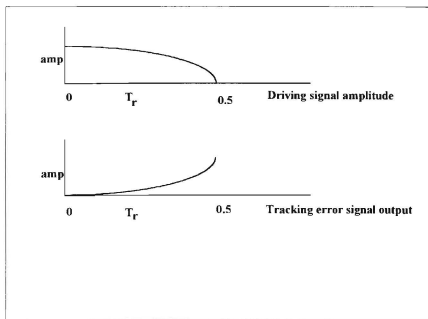


Figure 15. Con-Scan Seeker No Jamming Driving Signal.

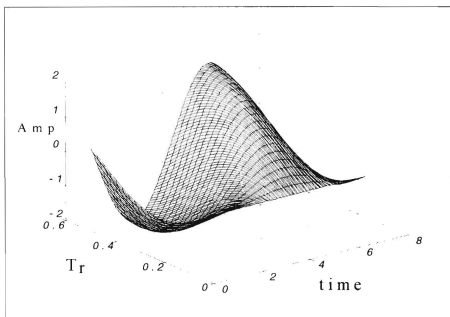


Figure 16-1 Con-Scan Seeker No Jamming Tracking Error Output.

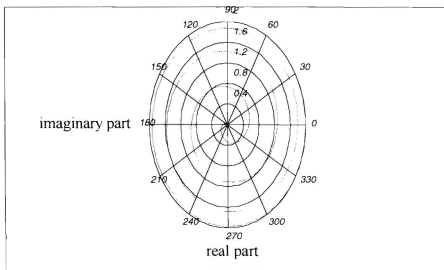


Figure 16-2 Con-Scan Seeker No Jamming Phasor Diagram.

This analysis is based on the large error case, in which the tracking error signal is developed from the nutation circle falling partly outside the reticle. The signal is developed as a function of T_r/T_m , the ratio of time on the reticle to total nutation cycle time. Thus there is no tracking error signal for the range $T_r/T_m=0$, in which the nutation circle is totally outside the reticle or for $T_r/T_m=1$, when it is totally inside. In the latter case track information must be determined from the carrier frequency modulation. However if the nutation circle is close to the reticle perimeter, $T_r/T_m=1$ is essentially the bore sighted condition. The strength of the tracking error signal is zero at both limits $T_r/T_m=0$ and $T_r/T_m=1$, and reaches a maximum at $T_r/T_m=0.5$. This is apparent in Figure 16-1. The phase angle provides the direction of the driving correction to target track.

E. CON-SCAN SEEKER UNDER ACTIVE IR JAMMING

1. Target And Jamming Signal Seen By The Seeker

To get an insight into the jammer and seeker interaction, one should define the reticle modulation function and jammer modulation function first. These are shown graphically in Figure 17 and can be represented by a Fourier series as shown in equation (52).

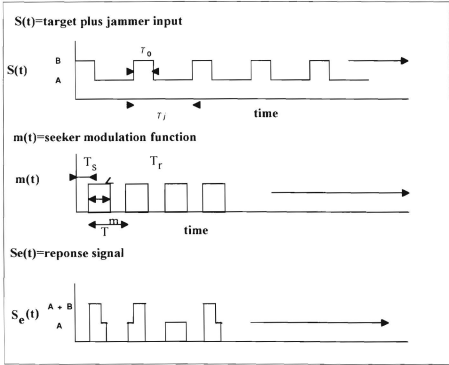


Figure 17. Con-Scan Seeker Effective Target And Jammer Waveforms

$$\text{Here } S(t) = A + \sum_{n=-\infty}^{\infty} c_n \exp(jn\omega_j t) \quad (52)$$

where

$$c_n = \frac{jB}{2\pi n} [\exp(-j2\pi n \frac{T_0}{T_j}) - 1] \quad (53)$$

A is the target radiation power, B is the jammer radiation power, T_0 is the jammer pulse duration, and T_j is the jammer waveform period ($\omega_j = 2\pi/T_j$), T_s is the phase delay of the target relative to the jammer modulation.

2. The Tracking Error Signal Output

Note that for simplification the carrier-signal generation is implicitly assumed and has been omitted from consideration. Also any nonlinearities (such as limiters) also have been ignored. For this reason, the inferences reached here may or may not be valid for specific con-scan seekers, depending on the details of their signal processing

From above one can derive the power to the detector, and hence the track error function $P(t)$, which can be written in the form:

$$P_d(t) = [A + \sum_{n=-\infty}^{\infty} c_n \exp(jn\omega_j t)] m(t) \quad (54)$$

where

$$m(t) = \sum_{n=-\infty}^{\infty} d_n \exp[jn\omega_m(t - T_s)] \quad (55)$$

and where

$$d_n = \frac{j}{2\pi n} [\exp(-j2\pi n \frac{T_r}{T_m}) - 1] \quad (56)$$

Here again we filter around the fundamental frequency, keeping only the $n=0$ $n=-1$ and $n=1$ terms to derive the response function, in the form

$$P_d(t) = \{A + \frac{jB}{2\pi} [2j \sin(\omega_j t - 2\pi \frac{T_0}{T_j}) - 2j \sin(\omega_j t)]\} \times \\ \{ \frac{T_r}{T_m} + \frac{j}{2\pi} [2j \sin(\omega_m(t - T_s) - 2\pi \frac{T_r}{T_m}) - 2j \sin(\omega_m(t - T_s))] \} \quad (57)$$

This gives us the envelope waveform

$$S_e(t) = (A + B \frac{T_0}{T_j}) \sin(\pi \frac{T_r}{T_m}) \cos(\omega_m t - 2\pi \frac{T_i}{T_m} - \pi \frac{T_r}{T_m}) \\ + B \frac{T_r}{T_m} \sin(\pi \frac{T_0}{T_j}) \cos(\omega_j t - \pi \frac{T_0}{T_j}) \quad (58)$$

Assuming that a scaled version of $S_e(t)$ is processed to represent the seeker torquing signal, the low-frequency component of its interaction with the spinning gyro magnet has the form:

$$S_e(t) = (A + B\frac{T_0}{T_j})\sin(\pi\frac{T_r}{T_m})\exp(j\pi(2\frac{T_s}{T_m} + \frac{T_r}{T_m}) + B\frac{T_r}{T_m}\sin(\pi\frac{T_0}{T_j})\exp[-j(\Delta\omega t - \pi\frac{T_0}{T_j})] \quad (59)$$

where $\Delta\omega = \omega_s - \omega_m$. In response to this drive signal, the seeker tracking loop will adjust T_r and T_s to keep the average seeker tracking error rate at zero.

Here we are going to discuss two different condition - jammer modulation at the reticle frequency, and jammer modulation different from reticle modulation frequency.

a. The Jammer Modulation Frequency Same As The Reticle Modulation Frequency

Here we must take into consideration both the real part and imaginary parts of the drive signal $S_e(t)$. The driving signal is tending to reduce the total tracking error to zero. The complex track error rate function gives two conditions needed to reach zero rate: the two terms in $S_e(t)$ will completely cancel if their magnitudes are equal and their phases differ by π radians, so in the real part of $S_e(t)$ we should let the magnitudes be equal:

$$(A + B\frac{T_0}{T_j})\sin(\pi\frac{T_r}{T_m}) - B\frac{T_r}{T_m}\sin(\pi\frac{T_0}{T_j}) = 0 \quad (60)$$

then the phase of the two terms must be set to have a difference of 180 degree, so that

$$\frac{T_s}{T_m} = \frac{1}{2}(\frac{T_0}{T_j} - \frac{T_r}{T_m} + 1) \quad (61)$$

By satisfying both of these two function we can get the tracking error output signal equal to zero. However, the driving signal has already taken both jammer and target combined signal into consideration, so that the driving signal will adjust T_s and T_r to fulfill the goal. This will cause miss track because the driving signal will adjust T_s then the phase angle (target direction) will incorporate these values to apply the correction in the wrong direction. The effect on T_s is illustrated in Figure 18.

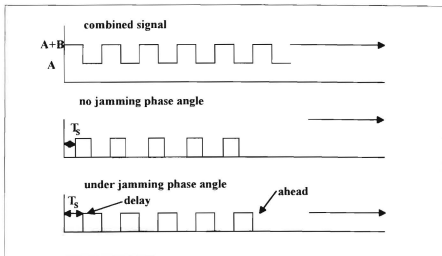


Figure 18. Con-Scan Seeker Under Jamming Phase Angle Deception Condition.

From the above diagram we can see the phase angle has been stolen, also the T_r part has been modified by jamming, i.e., the driving signal pulled the seeker to another direction and the strength is different from the no jamming condition.

b. The Jammer Modulation Frequency Different From The Reticle Modulation Frequency

When the jammer modulation frequency is different from the reticle modulation frequency the jamming result not only depends on the jamming ratio, and the fraction of time on reticle, but also depends on the frequency difference between the jammer modulation and reticle modulation. This will cause the tracking error to be more unstable.

Following part a we see that the seeker-torquing signal will adjust T_s and T_r to seek the equilibrium point when we give a jamming ratio, so the feedback loop only depends on the jamming ratio to make another adjustment. Here we add another coefficient, the modulation frequency ω_m , to jamming of the con-scan seeker. This will impact on the phase term and cause the target position change to depend on the difference frequency. The amplitude and phase conditions of the previous page are changed only by addition of the difference frequency $\Delta\omega = \omega_j - \omega_m$ in the phase.

In the real part we should let the magnitude equal

$$(A + B \frac{T_0}{T_j}) \sin(\pi \frac{T_r}{T_m}) - B \frac{T_r}{T_m} \sin(\pi \frac{T_0}{T_j}) = 0 \quad (62)$$

in the phase condition we should set the phase difference as 180 degrees

$$\text{i.e. } \frac{T_s}{T_m} = \frac{1}{2} (\Delta\omega t - \pi \frac{T_0}{T_j} - \frac{T_r}{T_m}) \quad (63)$$

The tracking error will adjust to an equilibrium condition depending on the target time on the reticle and the jamming ratio and apply the two values to the phase term to determine the phase angle (new apparent target position). Those values should meet the requirement of tracking error output equal to zero. Under this condition the tracking loop will be more complicated than the condition of part a. The two conditions treated are shown as Figures 19-1 and 19-2. We also show the tracking error

output signal phasor diagram in Figures 20-1 and 20-2. A sample of simulation program is shown as appendix.

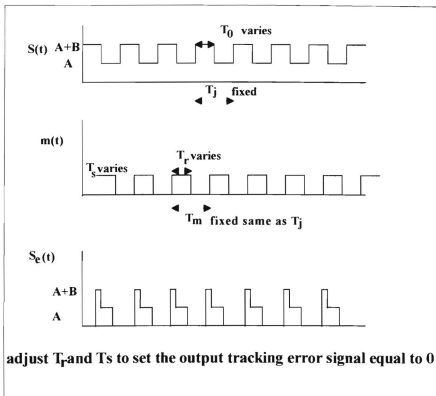


Figure 19-1. Con-Scan Seeker Under Active Ir Jamming Jammer And Seeker Modulation Frequencies Fixed And Equal

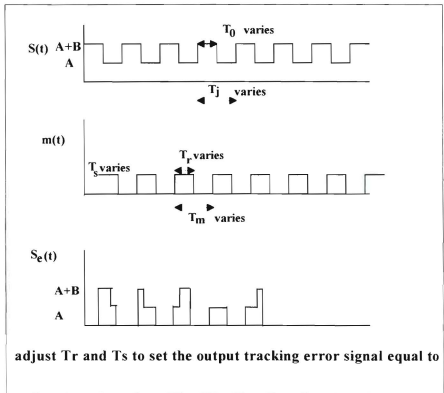


Figure 19-2. Con-Scan Seeker Under Active Ir Jamming. Jammer And Seeker Modulation Frequencies Varied

Figures 19-1 and 19-2 show schematically that when the modulation frequency varies then the T_r and T_s should adjust frequently since all the input all varies in time. It follows that the tracking error rate not only provides false tracking information but also change rapidly.

The first simulation is conducted with jammer power B and modulation frequency ω_j fixed but with the phase delay of the jammer varied in time. The phasor diagram of the tracking error rate is shown in Figure 20-1.

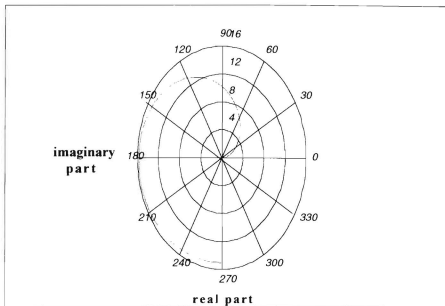


Figure 20-1. Con-Scan Seeker With Active Ircm Phasor Diagram Of Track Error Rate

Comparing the phasor diagram with that for no jamming we see that the real part of the tracking error output is 10 times bigger than with no jamming, the phase angle (target position) also is different from the no jamming condition, and the rotation rate is slower than with no jamming. The jamming effectiveness is not dependent on the modulation frequency but only on the jamming ratio.

The second simulation is conducted with jammer power fixed, modulation frequency varied and the phase delay of the jammer time varying. The phasor diagram of the tracking error rate is shown in Figure 20-2.

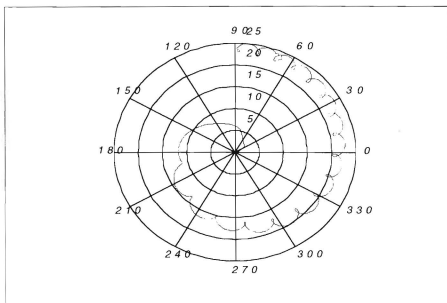


Figure 20-2 Con-Scan Seeker Under Jamming. Jammer Modulation Frequency
Different From The Reticle Modulation Frequency.
Phasor Diagram Of Track Error Rate.

Comparing the phasor diagram of Figure 20-2 with that for jamming at the reticle modulation frequency, we see that the difference modulation frequency causes the real part of the tracking error output to vary rapidly. The phase angle (target position) shows a similar result, indicating that the jamming effect depends not only on the jamming ratio but also on the difference of modulation frequency.

F. CON-SCAN SEEKER UNDER FLARE JAMMING

Under the assumption the target radiation power should have a constant value and the flare power also have a constant value the total power seen by the seeker can be represented by a periodic signal, this is represented schematically in Figure 21.

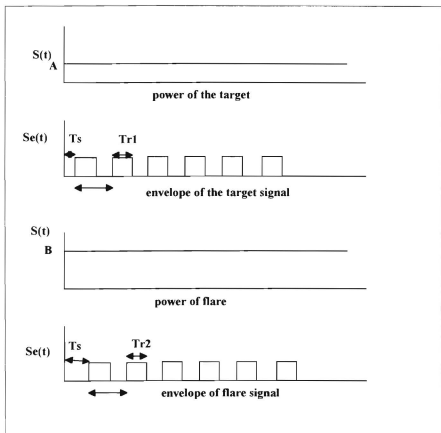


Figure 21. Con-Scan Seeker Under Flare Jamming.

To understand the interaction of the flare and target signals in the seeker, one must first define the reticle modulation function and jammer modulation function. Both can be represented by Fourier series.

The total power to the detectors can be written:

$$P_d(t) = A \left\{ \sum_{n=-\infty}^{\infty} d_n \exp[jn\omega_m t] \right\} + B \left\{ \sum_{n=-\infty}^{\infty} d_n \exp[jn\omega_m (t - T_s)] \right\} \quad (64)$$

where

$$d_n = \frac{j}{2\pi n} [\exp(-j2\pi n \frac{T_r}{T_m}) - 1] \quad (65)$$

The interaction diagram is shown as Figure 22.

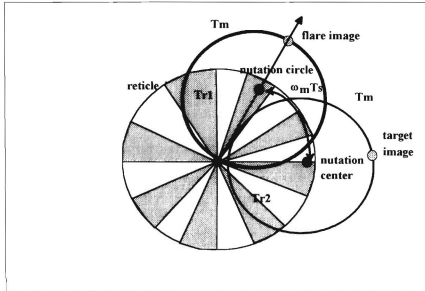


Figure 22. Con-Scan Seeker Under Flare Jamming. Schematic Of Interaction Of Flare And Target Images With Seeker Reticle.

From the power function $P_d(t)$ seen by the seeker we can derive the interaction function:

$$P_d(t) = A \{ d_0 + d_1 \exp(j\omega t) + d_{-1} \exp(-j\omega t) \} + B \{ d_0 + d_1 \exp(j\omega(t - T_s)) + d_{-1} \exp(-j\omega(t - T_s)) \} \quad (66)$$

From this the low frequency tracking error rate waveform follows as analogously to the previous case, as:

$$S_e(t) = \frac{A}{\pi} \sin \omega t + \frac{B}{\pi} \sin(\omega(t - T_s)) - \frac{A}{\pi} [\sin(\omega t - 2\pi \frac{T_{c1}}{T_m})] - \frac{B}{\pi} [\sin(\omega(t - T_s) - 2\pi \frac{T_{c2}}{T_m})] \quad (67)$$

From this tracking error rate output we can see that the time on reticle for target and flare will define the new tracking error magnitude and the phase delay will determine the new phase angle. The corresponding diagram of $S_e(t)$ against T/T_m and time delay are shown as Figures 23-1 and 23-2. Figure 23-3 shows the phasor diagram representation of the track error rate.

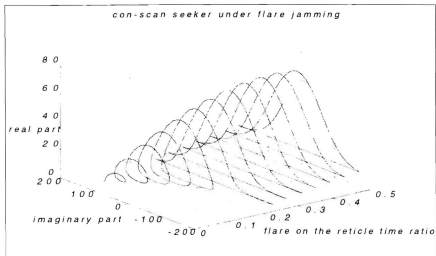


Figure 23-1. Con-Scan Seeker Under Flare Jamming 3D Diagram Of Track Error Rate Versus T_r/T_m For Flare.

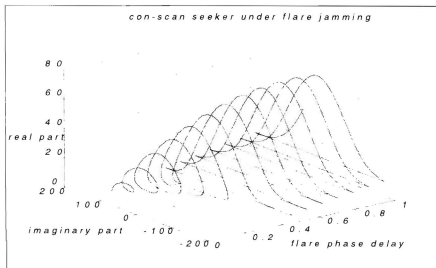


Figure 23-2. Con-Scan Seeker Under Flare Jamming. Phase Delay 3D Diagram.

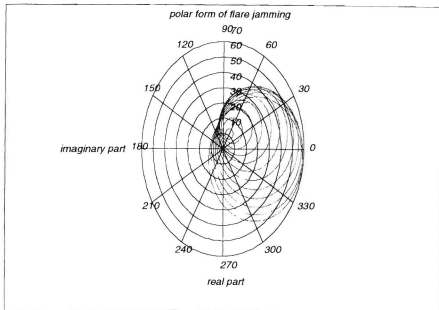


Figure 23-3. Con-Scan Seeker Under Flare Jamming. Phasor Diagram Of Track Error Rate.

From these simulation diagrams we can see that when the flare power entering the reticle is small then the impact on the tracking error rate will small, when the flare power into the reticle is larger then the tracking error rate output will increase. The tracking error output under flare jamming can be effective in reducing the seeker tracking accuracy.

The phase term shows that when the flare leaves the target it will provide a phase difference which will cause the seeker to recompute the apparent position. This will cause the seeker to track in the wrong direction, giving the required countermeasure effectiveness.

G. COMMENT AND RESULT

For the con-scan seeker case we simulated performance under no jamming, under active IR jamming and Flare jamming conditions. For the active IR jammer, the jammer is collocated with the target, so the false target image and the real target image will be seen by the seeker in the same location (same α), In discussing jamming the missile seeker one should take the jammer time on reticle (power) and the jamming modulation frequency into consideration. When the jamming modulation frequency is the same as the target modulation frequency the tracking error output in trying to keep it at the equilibrium point it will adjust not only the time on reticle but also the phase delay. Thus the phase delay will be the important parameter in determine the jamming effectiveness (wrong target position indication).

The jamming power requirement, depend not only on the jamming power but also on the jammer time-on-reticle coefficient T_r ; this will change the jammer power seen by the seeker. When the jamming modulation frequency is different from the target modulation frequency, the power seen by the reticle will depend on both modulation frequencies. The tracking error rate output will then adjust the phase delay to find an equilibrium point. In order to break-lock the missile seeker, correct control of the jammer modulation frequency and the power can lead to a high probability to break-lock the missile.

In the flare case, since the flare separates from the aircraft, this provide the target-flare phase difference and power into the seeker, so we only need to consider target and flare separation speed. Once we find the trajectory of the flare and the aircraft moving moment then we can determine whether the flare can break-lock the missile or not. From the simulation plots, under the appropriate conditions, if the phase angle is sufficiently different from the no jamming condition, the flare has high probability to break-lock the missile.

The theoretical analysis indicates that the simplified case of a con-scan seeker under large error conditions can be successfully jammed by the active IR jammer and flare. The analysis done here is only a paper study; one should evaluate it in operational testing to ensure its validity, and the evaluation must extend to application against different types of con-scan seeker.

VII. CONCLUSION

To reduce the IR missile (spin-scan and con-scan seeker) kill probability, active IR jammers and Flares are often employed against the missile guidance seeker. An active IR jammer and Flare may be able to degrade the accuracy of angular information developed by the seeker and may, therefore, greatly reduce the kill probability. In some cases, it may be able to cause break-lock of the tracking missile seeker causing it to become completely unlocked from the target. The missile must then reacquire its target and valuable time is lost, along with a great deal of information about the target position.

A theoretical analysis applied to an encounter simulation seems to indicate that it is possible to use the infrared jammer and flare to defeat the spin-scan and con-scan infrared missiles. The theoretical analysis of a simplified case of a spin-scan and con-scan reticle with amplitude modulation and frequency jamming leads to expressions for the target position, as seen by the missile seeker, under jamming and no jamming conditions. The jamming case is dealt with by theoretical and numerical analysis for a selected, non-optimal situation, as the closed form solution is not immediately apparent. The analysis indicates successful jamming in the situation studied. In the scenario where the infrared missile is an almost continuous threat during the aircraft's flight, the infrared jammer and the flare are short-term solutions that are potentially useful in increasing the survivability of these aircraft by reducing their susceptibility to infrared missile kills.

APPENDIX.[A SAMPLE OF THE SIMULATION PROGRAM]

Jammer power fixed and modulation frequency changed. Spin-scan seeker under active IR jamming. Target keep a constant IR signature. Active IR jammer keep a constant IR jamming power. Retical modulation frequency keep fixed. IR jammer modulation frequency changed

```
A=15;
B=26;
a=0.5;
t=0:0.001:7;
f1=10;
wm=(2*pi*f1);
f2=9:0.001:16;
wj=(2*pi*f2);
phai=0.5;
beta=(wm-wj). *t+phai;
x=a*(A+B/4)+B/2*(1+a/2) *exp(j*beta);
y=abs(x);
z=angle(x);
p=z*(180/pi);

plot3(f2,p,y),grid
title('spin-scan seeker under IR jammer jamming')
xlabel('jammer modulation frequency')
ylabel('the image part')
zlabel('the real part')
pause

polar(z,y);
grid;
title('polar form of ACTIVE IR jamming')
xlabel('the real part')
ylabel('the image part')
```

Power fixed and jammer modulation frequency changed. Con-scan seeker under active IR jamming. Target keep a constant IR signature. Active IR jammer keep a constant IR jamming power. Retical modulation frequency keep fixed. IR jammer modulation frequency changed.

```

A=15;
B=15;
pj=0.1:0.00005:0.6;
pm=0.0:0.00005:0.5;
ps=0.0:0.0001:1;
wm=80;
wj=70:0.002:90;
t=0:0.001:10;
k=(A+B*pj). *sin(pi*pm). *exp(j*pi*(2*ps+pm))+B *pm. *sin(pi*pj). *exp(-j*((wm-wj) *t)-
pi*pj);
y=abs(k);
z=angle(k);
p=z*(180/pi);
polar(z,y), grid

```

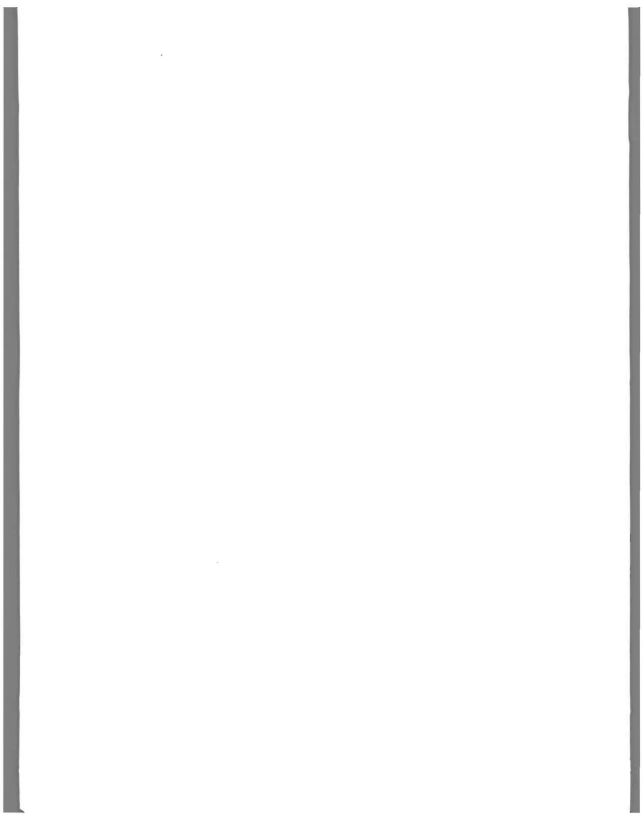
LIST OF REFERENCES

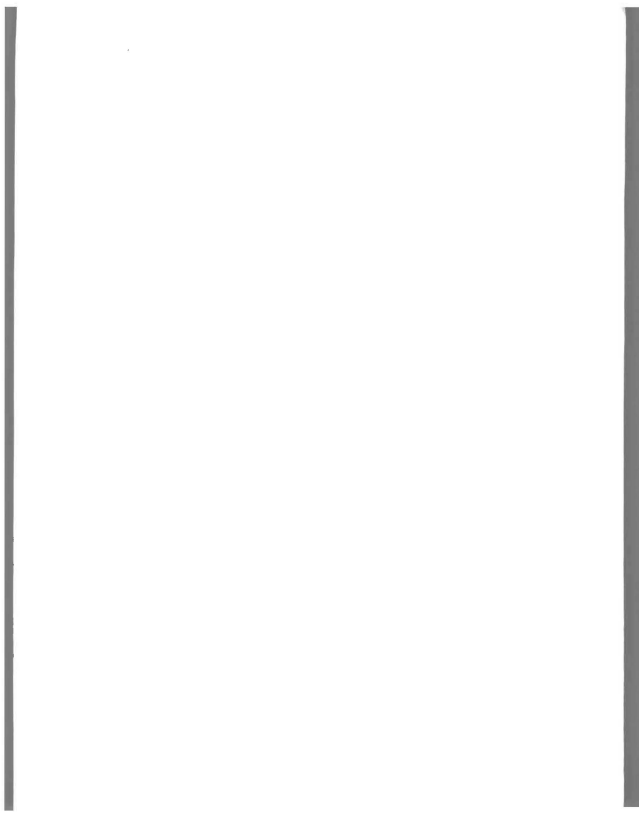
1. Charles J. Tranchita, Kazimieras Jackstas, Robert G. Palazzo, Joseph C. O'Connell *Active Infrared Countermeasures* The Infrared & Electro-Optical Systems Handbook Volume 7 Chapter Tree ERIM/SPIE PRESS, 1993.
2. Cooper, A. W., *Electro-Optic Devices and Principles*, Class notes for Ph3208 Course, Naval Postgraduate School, Monterey, 1993.
3. Cooper, A. W., *Electro-Optics/IR Systems and Countermeasures*, Class notes for Ph4209 Course, Naval Postgraduate School, Monterey, 1994.
4. Ball, Robert E. *The Fundamentals of Aircraft Combat Survivability Analysis and Design, Chapter Five*, AIAA 1985
5. Richard Legault *Reticles* The Infrared & Electro-Optical Systems Handbook Volume 3 Chapter Nine ERIM/SPIE PRESS, 1993.
6. Neal Brune *Expendable Decoys* The Infrared & Electro-Optical Systems Handbook Volume 7 Chapter Four" ERIM/SPIE PRESS, 1993.
7. Richard D. Hudson, JR *Infrared System Engineering* John Wiley & Sons, Inc., 1969.
8. Chia, Hock Teck *Reducing The Susceptibility Of Low Speed/ Low Maneuverability Aircraft To Infrared Missile Kills* MS Thesis, Naval Postgraduate School 1989.

9. Joseph S. Accetta *Infrared Search and Track System* The Infrared & Electro-Optical Systems Handbook Volume 5 Chapter Four ERIM/SPIE PRESS, 1993.

INITIAL DISTRIBUTION LIST

- | | | |
|----|---|---|
| 1. | Defence Technical Information Center
Cameron Station
Alexandria, Virginia 22304-6145 | 2 |
| 2. | Library, Code 52
Naval Postgraduate School
Monterey, California 93943-5000 | 2 |
| 3. | Electronic Warfare Academic Group
(Attn Prof.Frederic H. Levien, Code EC/LV)
Naval Postgraduate School
Monterey, California 93943-5000 | 1 |
| 4. | Prof.A.W.Cooper, Code Ph/Cr
Naval Postgraduate School
Monterey, California 93943-5000 | 3 |
| 5. | Prof.R.J.Pieper, Code EC/Pr
Naval Postgraduate School
Monterey, California 93943-5000 | 1 |
| 6. | Chinese Air Force Academy, Library
P.O.Box. 90277, Kang-Shan
Kau-Shong County, Taiwan, R.O.C | 1 |
| 7. | Chinese Air Force Headquarter, Weapon System Acquisition Div.
P.O.Box. 90251, Taipei
Taipei City, Taiwan, R.O.C | 1 |
| 8. | Chang,Ting Li
11, lane 84, Chao-Sin Rd, Sin-Dan.
Taipei County, Taiwan, R.O.C | 1 |







DUDLEY KNOX LIBRARY
NAVAL POSTGRADUATE SCHOOL
MONTEREY CA 93943-5101

GAYLORD 5

DUDLEY KNOX LIBRARY



3 2768 00100820 4